Electronic Supplementary Material (ESI) for Journal of Materials Chemistry A.

Supplementary Information

Controllable proton conducting pathways via situating polyoxometalates in targeting pores of a metal-organic framework

Xuying Lai,‡[a] Yiwei Liu,‡[a] Guocheng Yang,[b] Shumei Liu,[a] Zhan Shi,[c] Ying Lu,[a] Fang Luo[a] and Shuxia Liu*[a]

[a] Key Laboratory of Polyoxometalate Science of the Ministry of Education, College of Chemistry, Northeast Normal University, Changchun, Jilin 130024, China

[b] School of Chemistry and Life Science, Changchun University of Technology, Changchun, Jilin 130012, China

[c] State Key Laboratory of Inorganic Synthesis and Preparative Chemistry, College of Chemistry, Jilin University, Changchun, Jilin 130012, China

* Corresponding author: liusx@nenu.edu.cn.

‡ These authors contributed equally to this work.

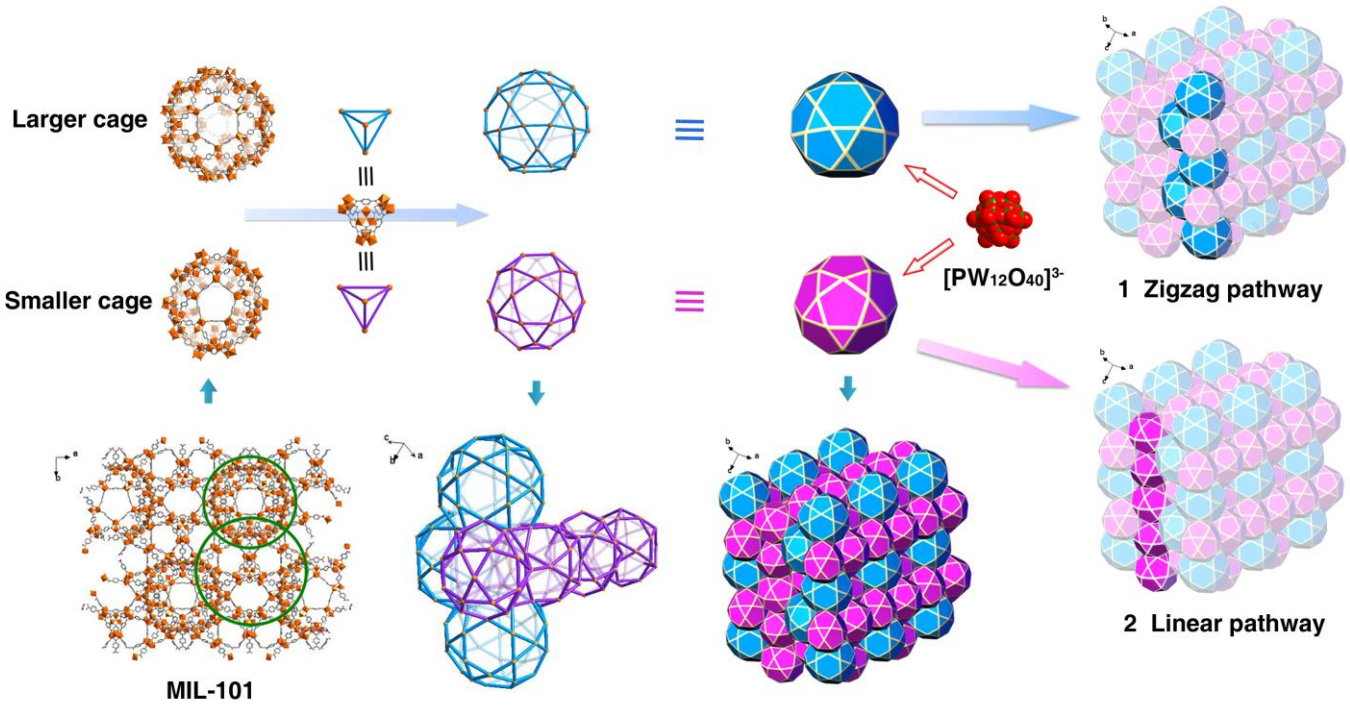

Figure S1. Structural and tiling representation of MIL-101 displaying coexistent two types of tunnels. Two types of proton conducting pathways were obtained by loading HPW into one of the two kinds of cages in MIL-101, respectively.

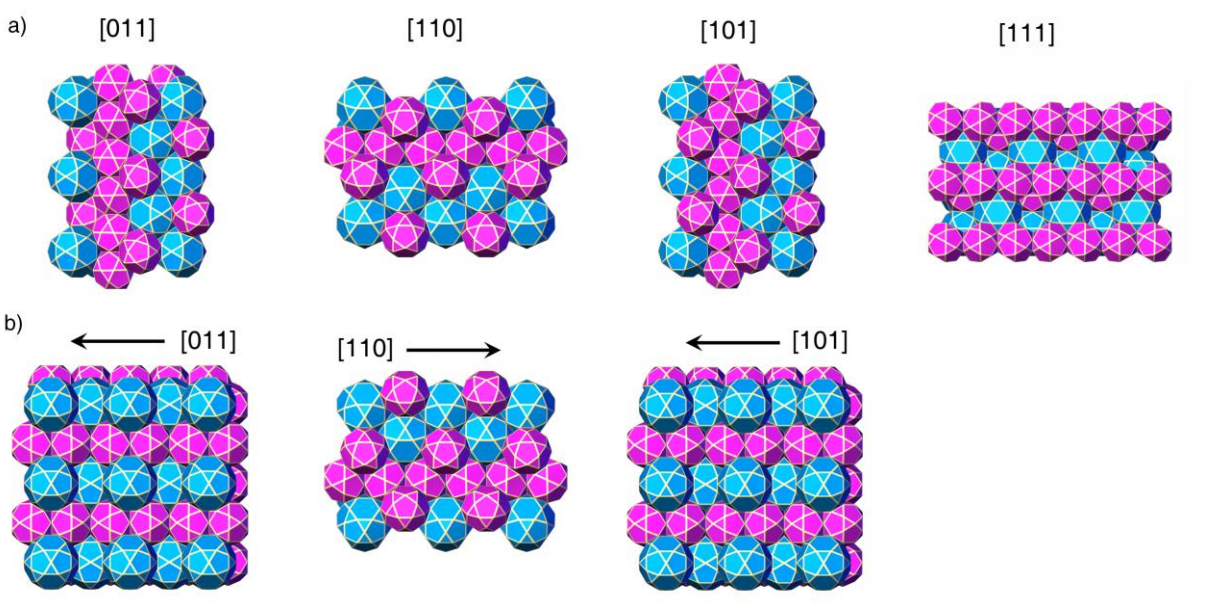

Figure S2. Zigzag and linear tunnels respectively constructed by larger and smaller cages are always arranged in parallel not only a) within [011], [110], [101], and [111] facets but also b) along [011], [110], and [101] facets orientation.

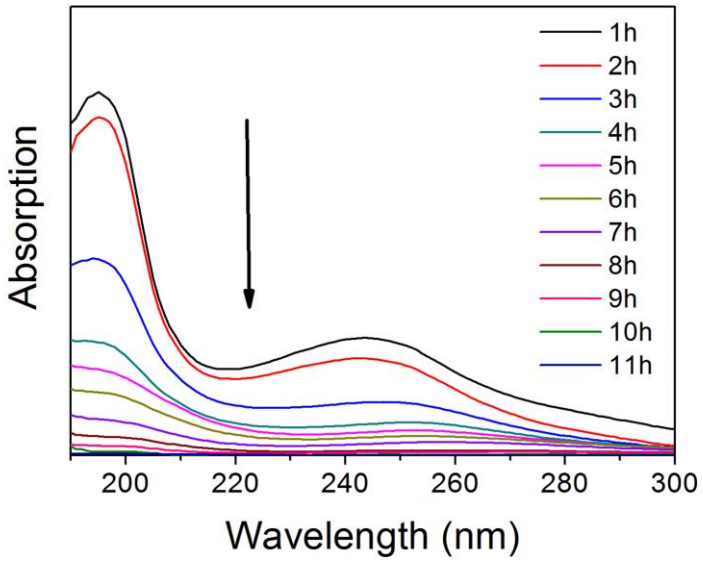

Figure S3. The UV–vis spectrum of HPW leaching from **3** each hour. **3** was suspended in water and the aqueous solution containing HPW was changed with deionized water and sampled each hour.

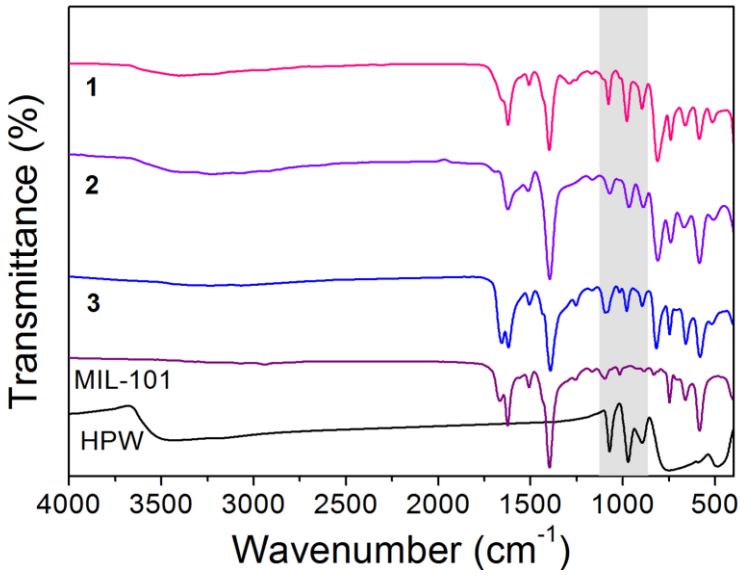

Figure S4. IR spectra of HPW (black), MIL-101 (purple), **1** (pink), **2** (light purple), and **3** (blue).

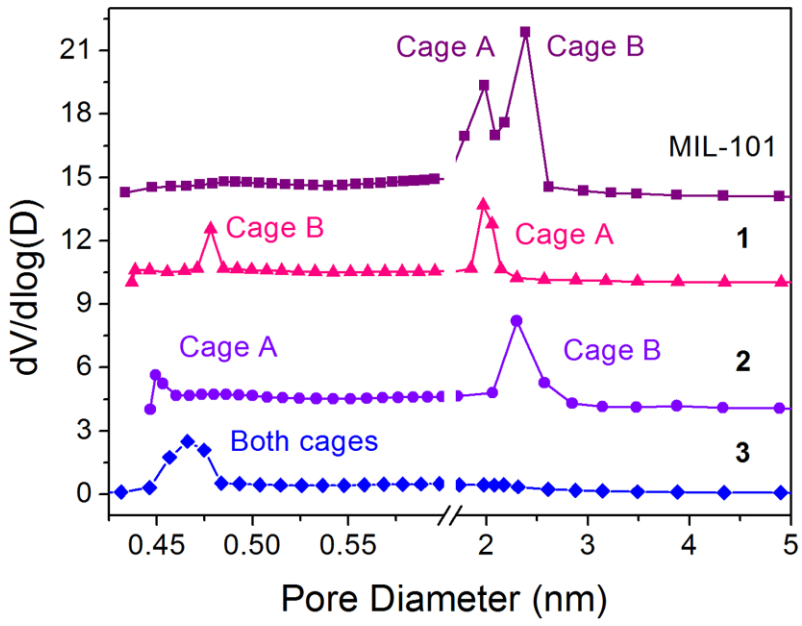

Figure S5. Pore size distributions for **1**-**3** and MIL-101.

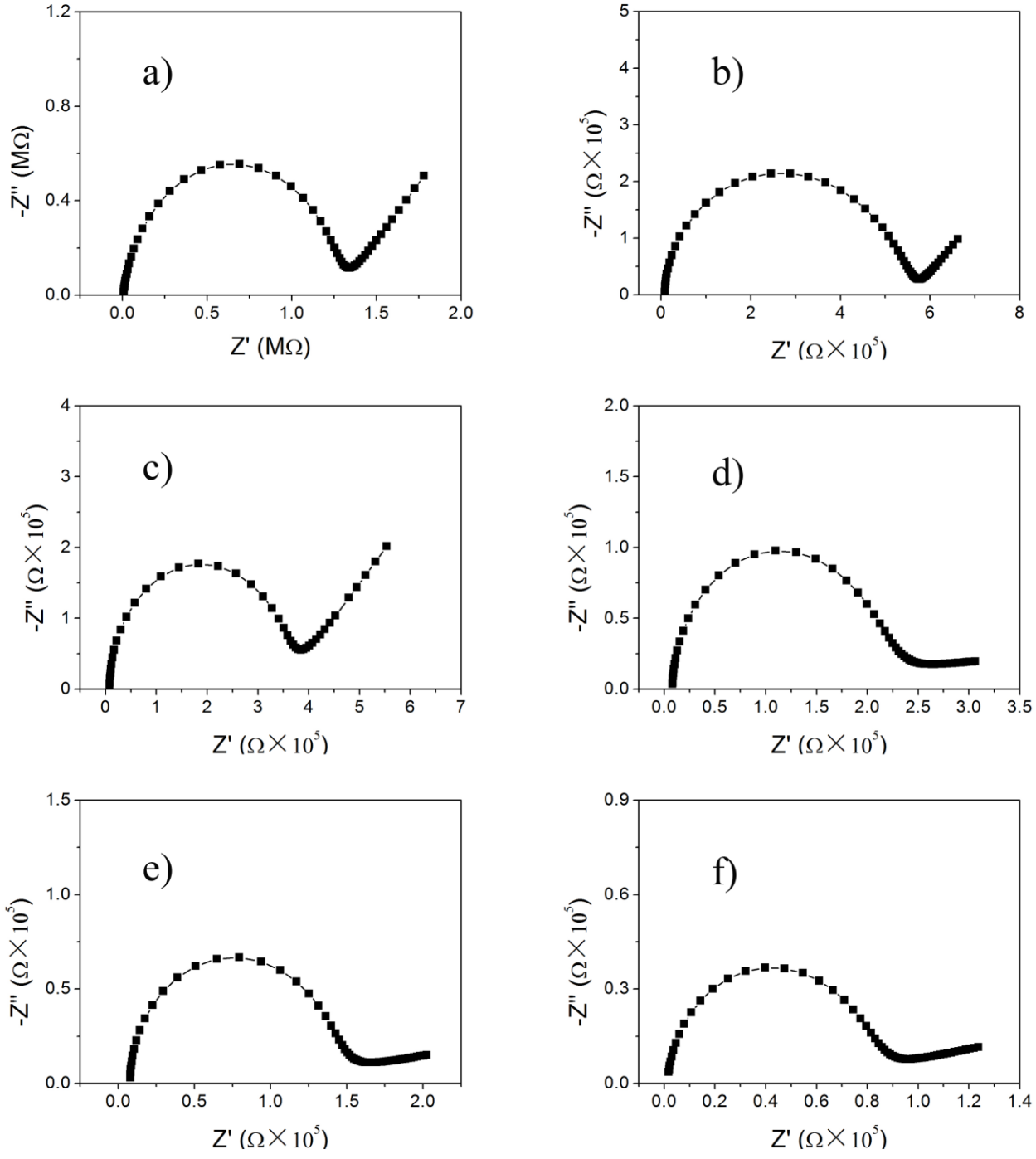

Figure S6. Nyquist plots of **1** at 100% RH and various temperatures (a) 25 °C, (b) 40 °C, (c) 50 °C, (d) 60 °C, (e) 70 °C, (f) 80 °C.

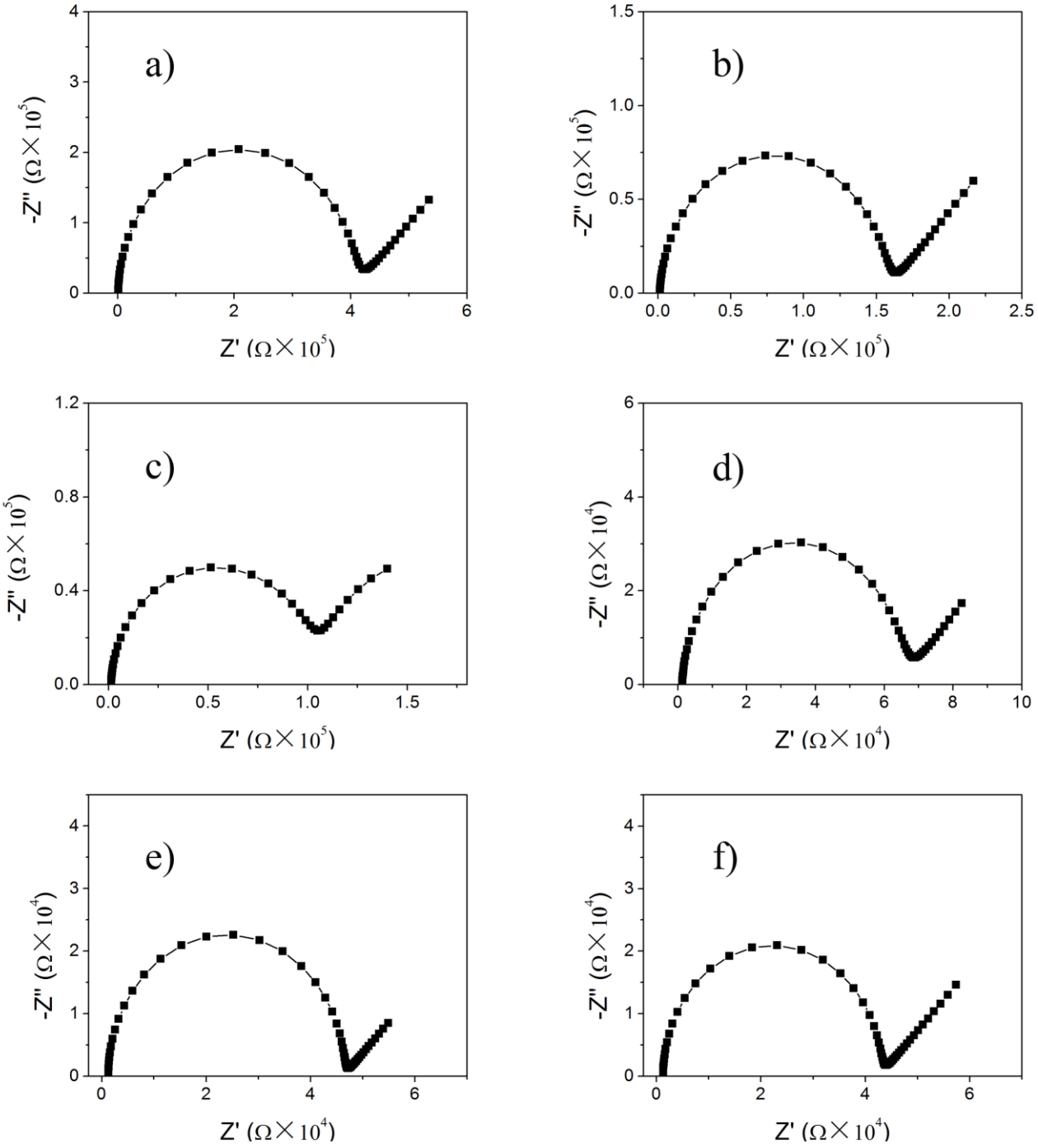

Figure S7. Nyquist plots of **2** at 100% RH and various temperatures (a) 25 °C, (b) 40 °C, (c) 50 °C, (d) 60 °C, (e) 70 °C, (f) 80 °C.

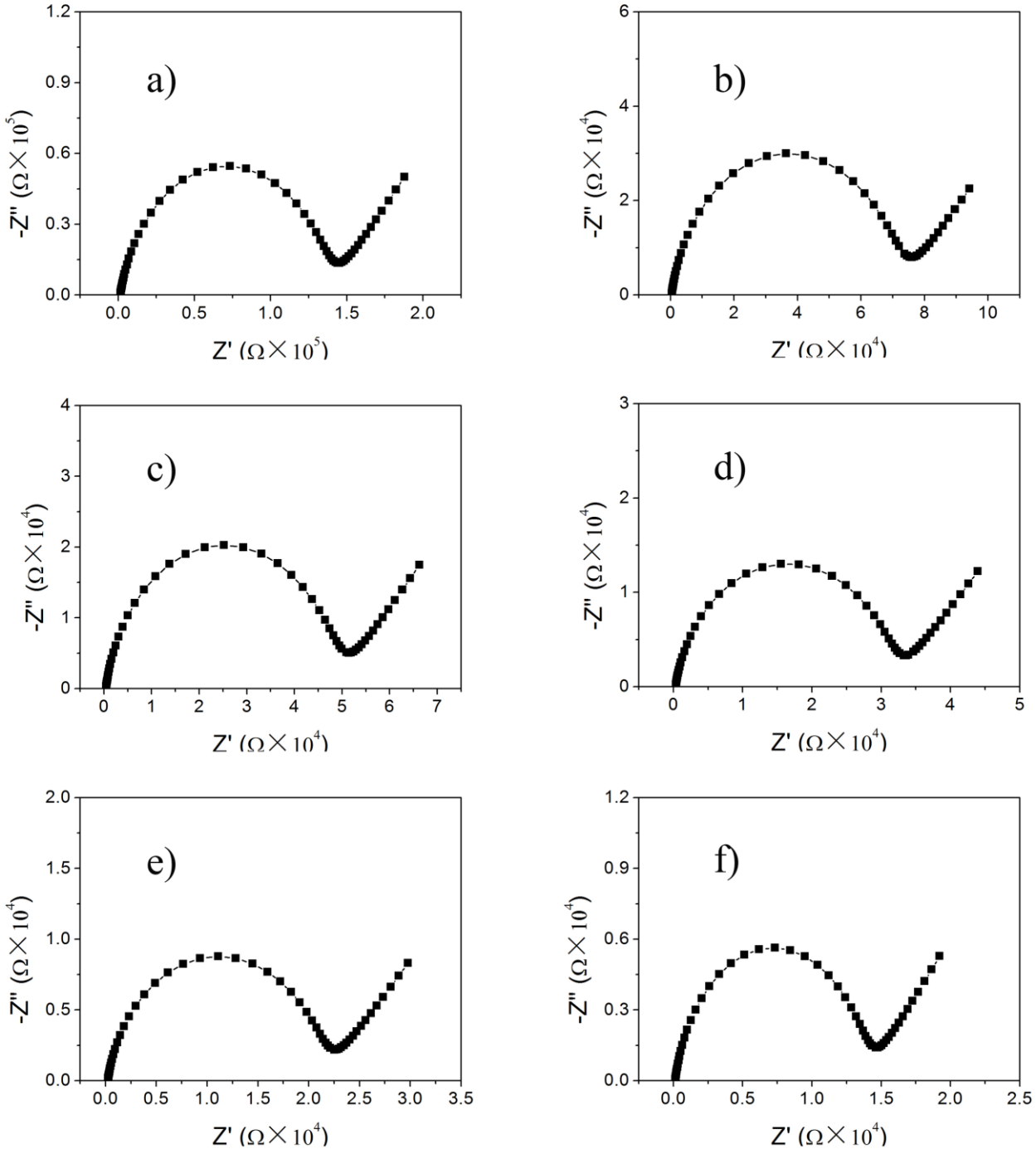

Figure S8. Nyquist plots of **3** at 100% RH and various temperatures (a) 25 °C, (b) 40 °C, (c) 50 °C, (d) 60 °C, (e) 70 °C, (f) 80°C.

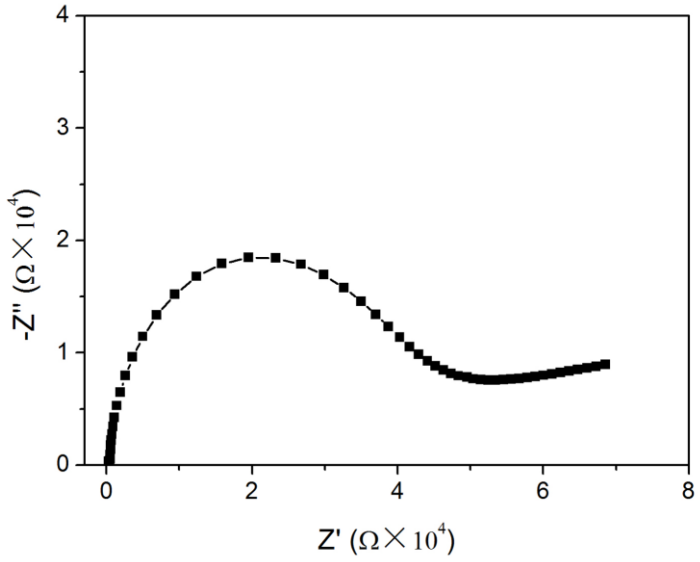

Figure S9. Nyquist plot of **2'** at 80°C 100% RH.

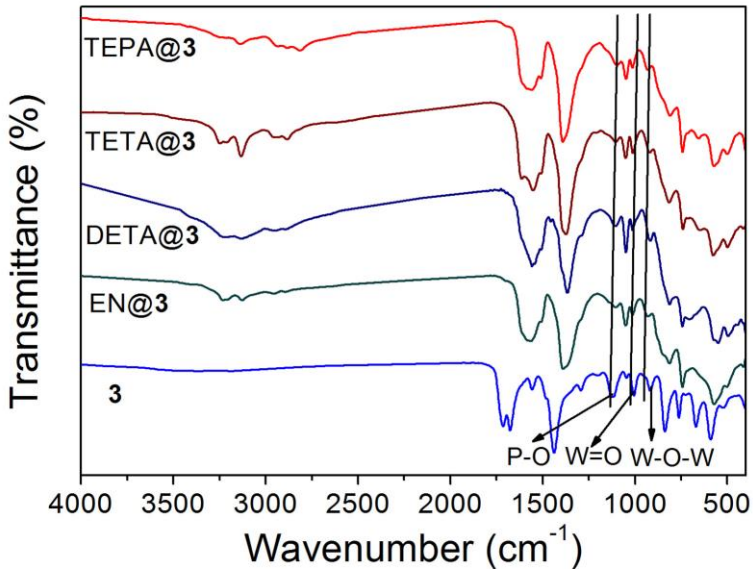

Figure S10. IR spectra of **3** (blue), EN@**3** (green), DETA@**3** (dark blue), TETA@**3** (dark red), and TEPA@**3** (red).

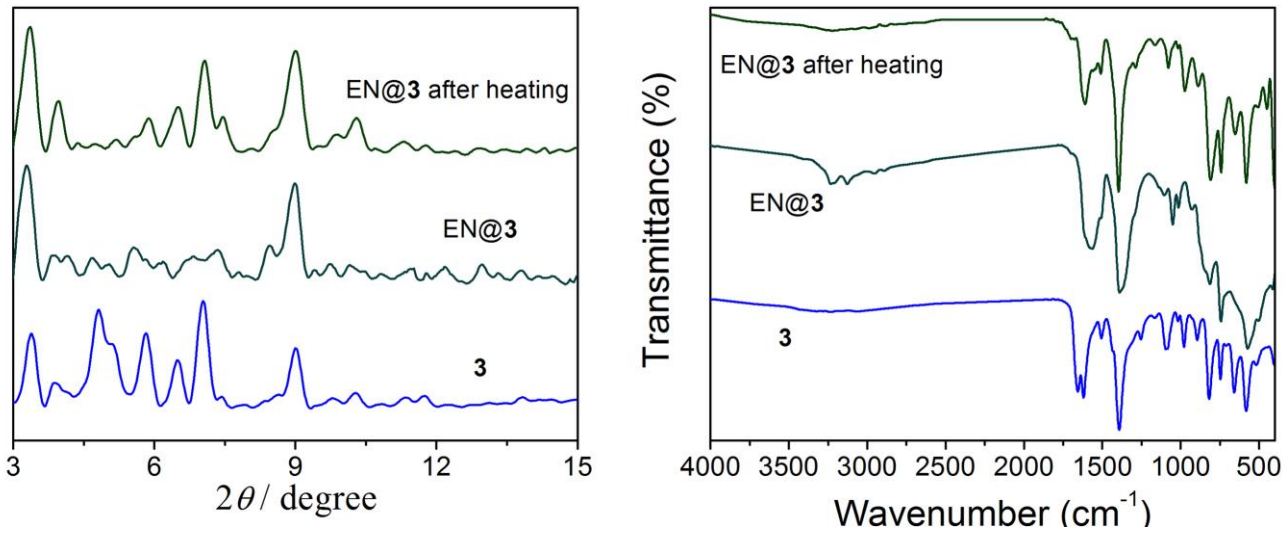

Figure S11. PXRD patterns (left) and IR spectra (right) of **3**, EN@**3**, and EN@**3** after heating for EN elimination.

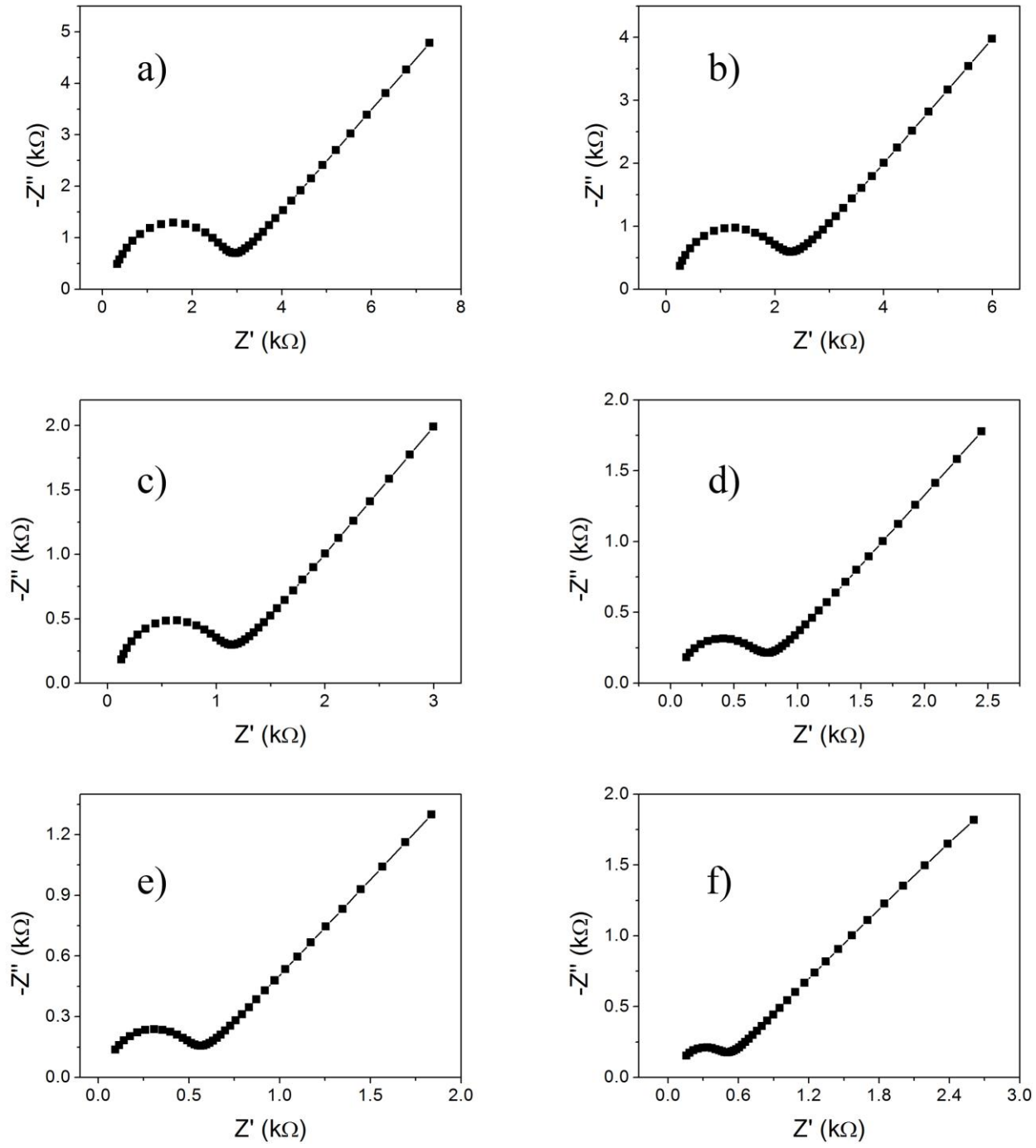

Figure S12. Nyquist plots of EN@**3** at 100% RH and various temperatures (a) 25 °C, (b) 40 °C, (c) 50 °C, (d) 60 °C, (e) 70 °C, (f) 80 °C.

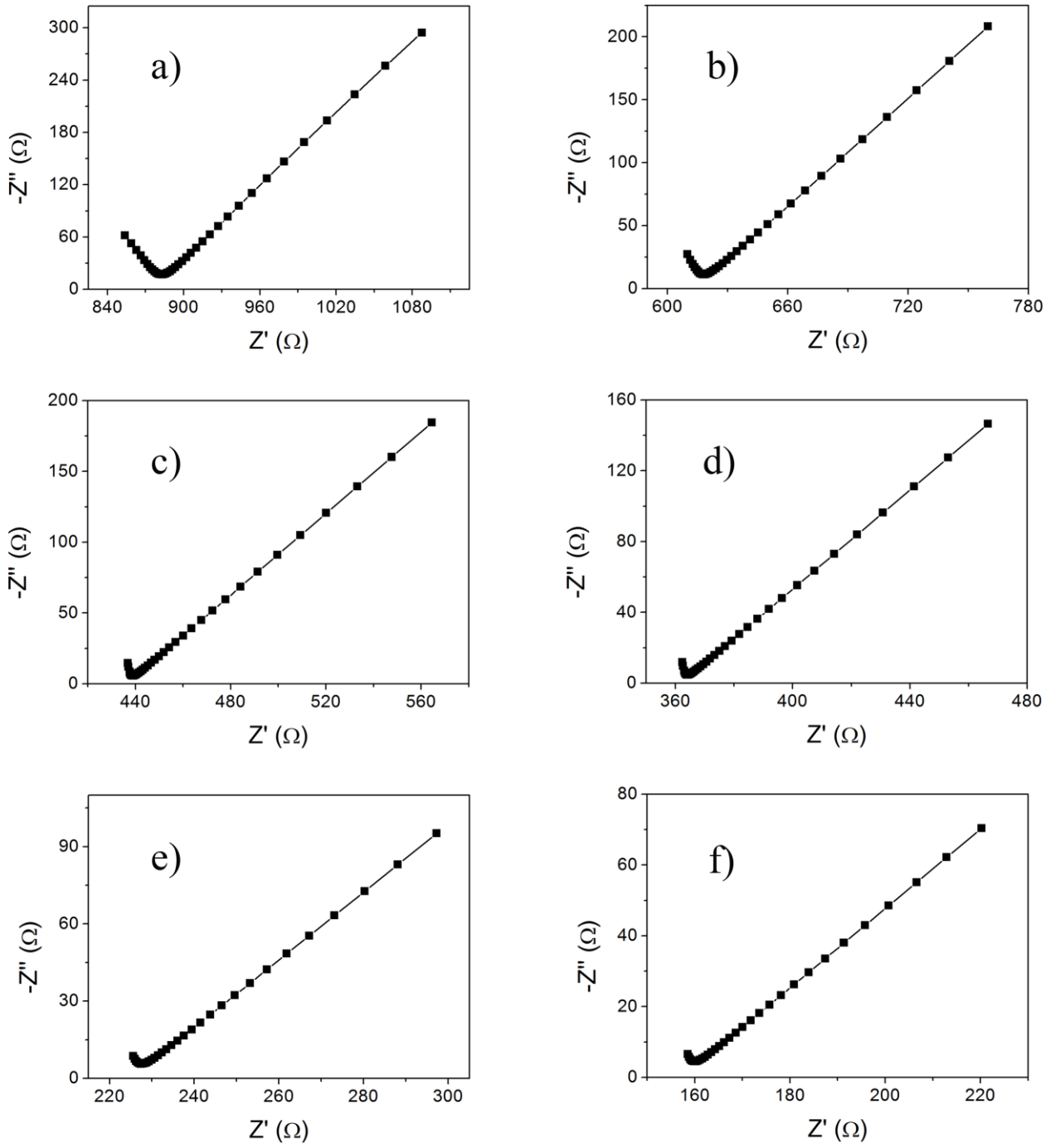

Figure S13. Nyquist plots of DETA@**3** at 100% RH and various temperatures (a) 25 °C, (b) 40 °C, (c) 50 °C, (d) 60 °C, (e) 70 °C, (f) 80 °C.

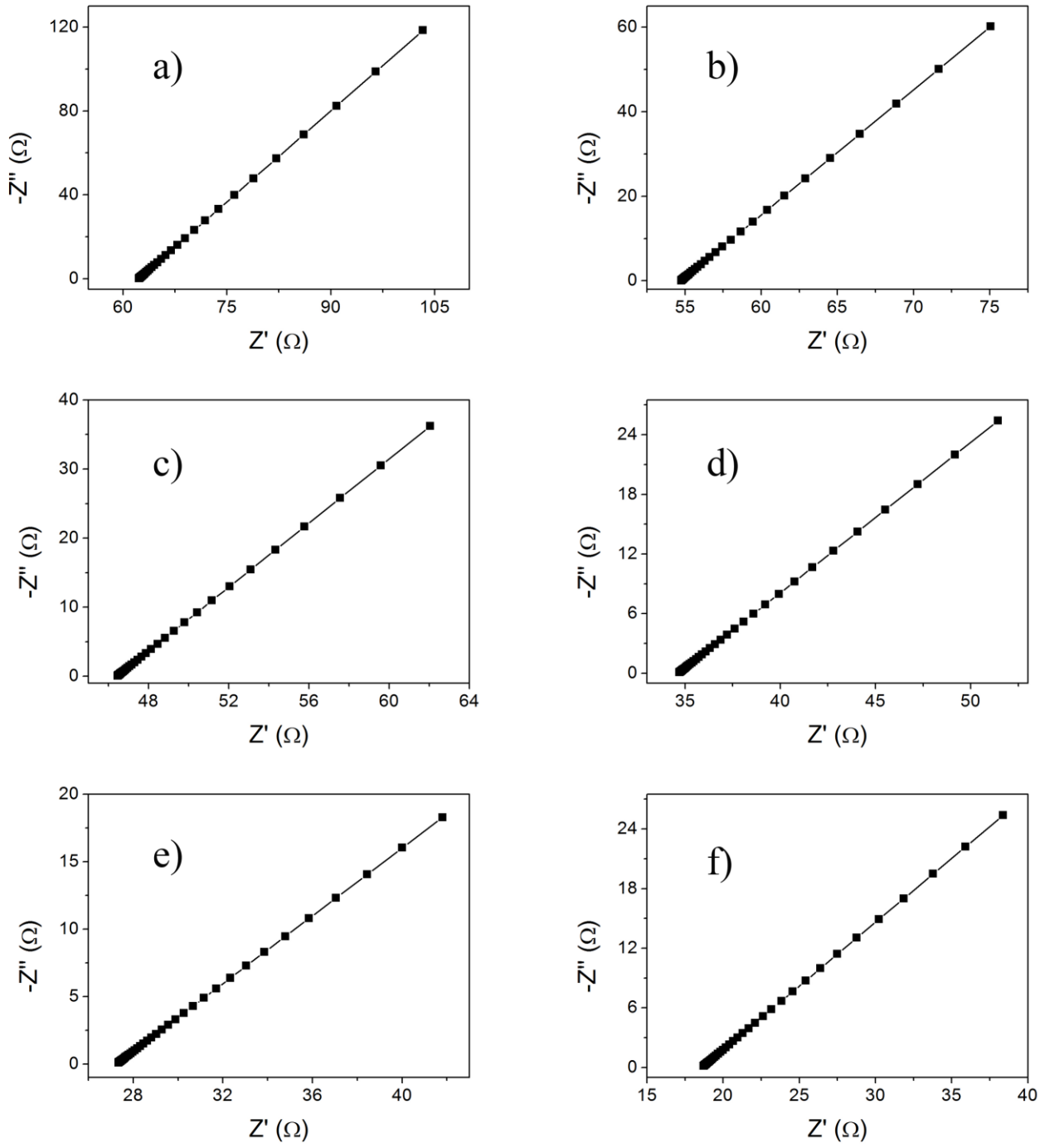

Figure S14. Nyquist plots of TETA@**3** at 100% RH and various temperatures (a) 25 °C, (b) 40 °C, (c) 50 °C, (d) 60 °C, (e) 70 °C, (f) 80 °C.

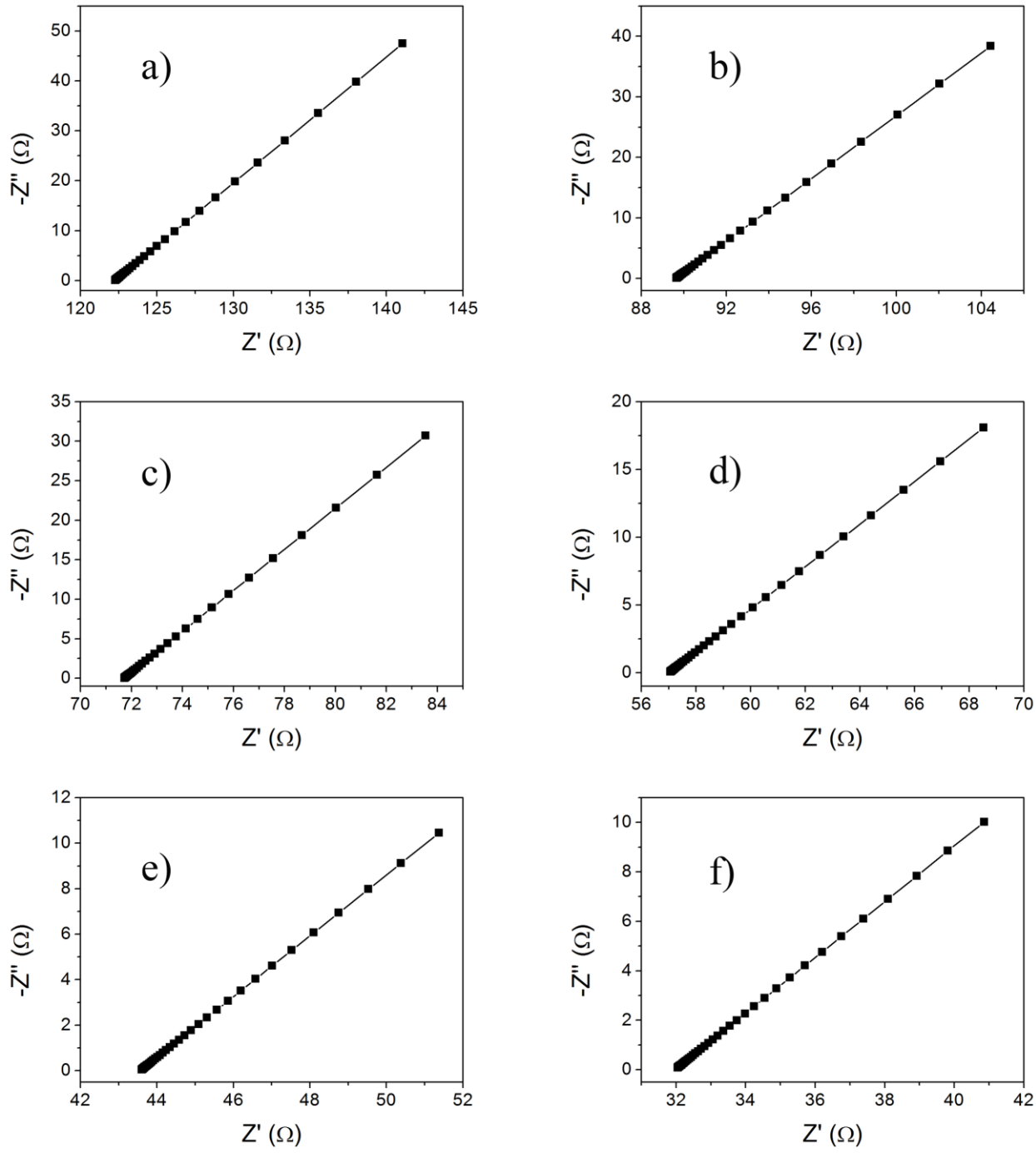

Figure S15. Nyquist plots of TEPA@**3** at 100% RH and various temperatures (a) 25 °C, (b) 40 °C, (c) 50 °C, (d) 60 °C, (e) 70 °C, (f) 80 °C.

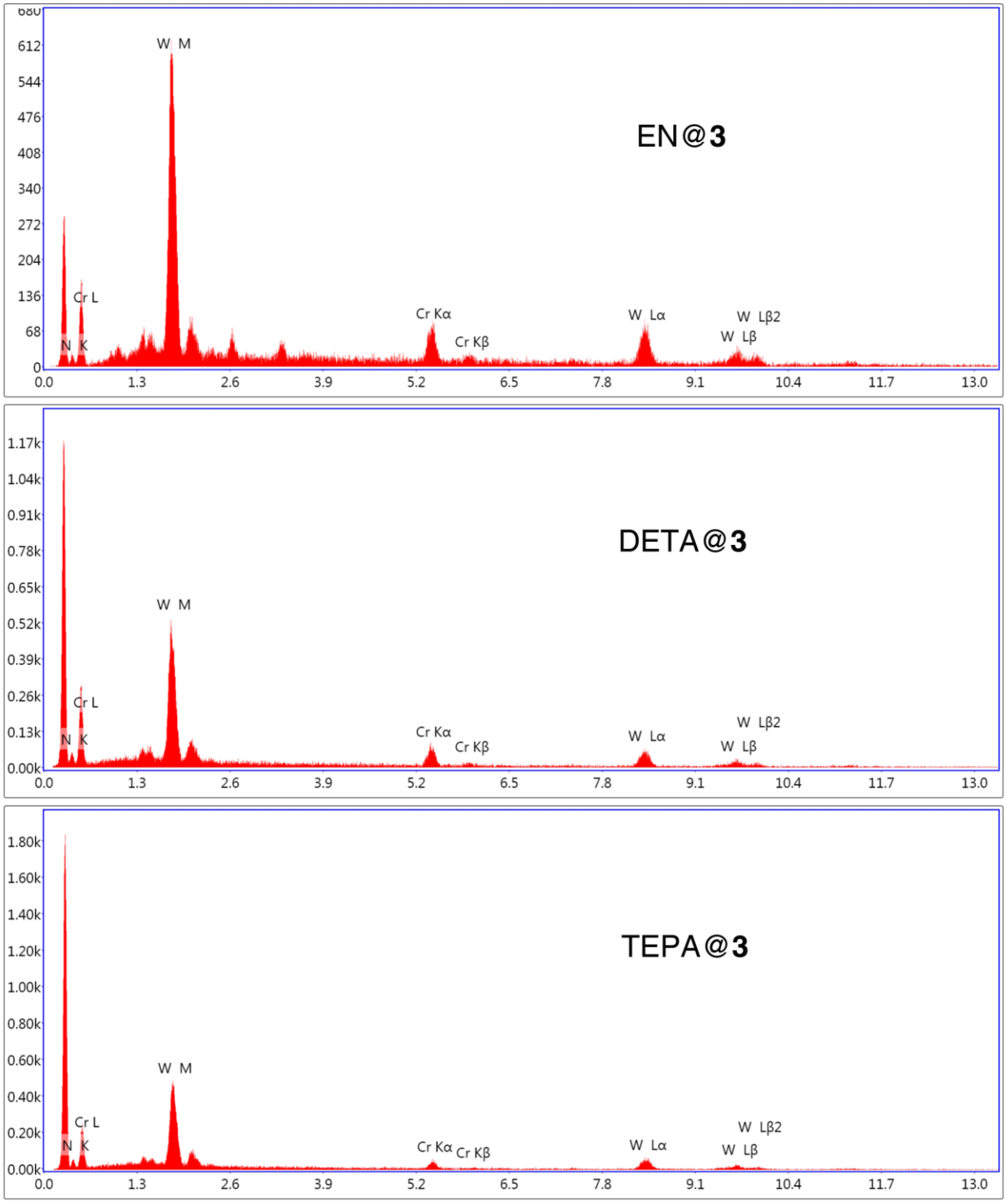

Figure S16. EDX spectrums for EN@**3**, DETA@**3**, and TEPA@**3**.

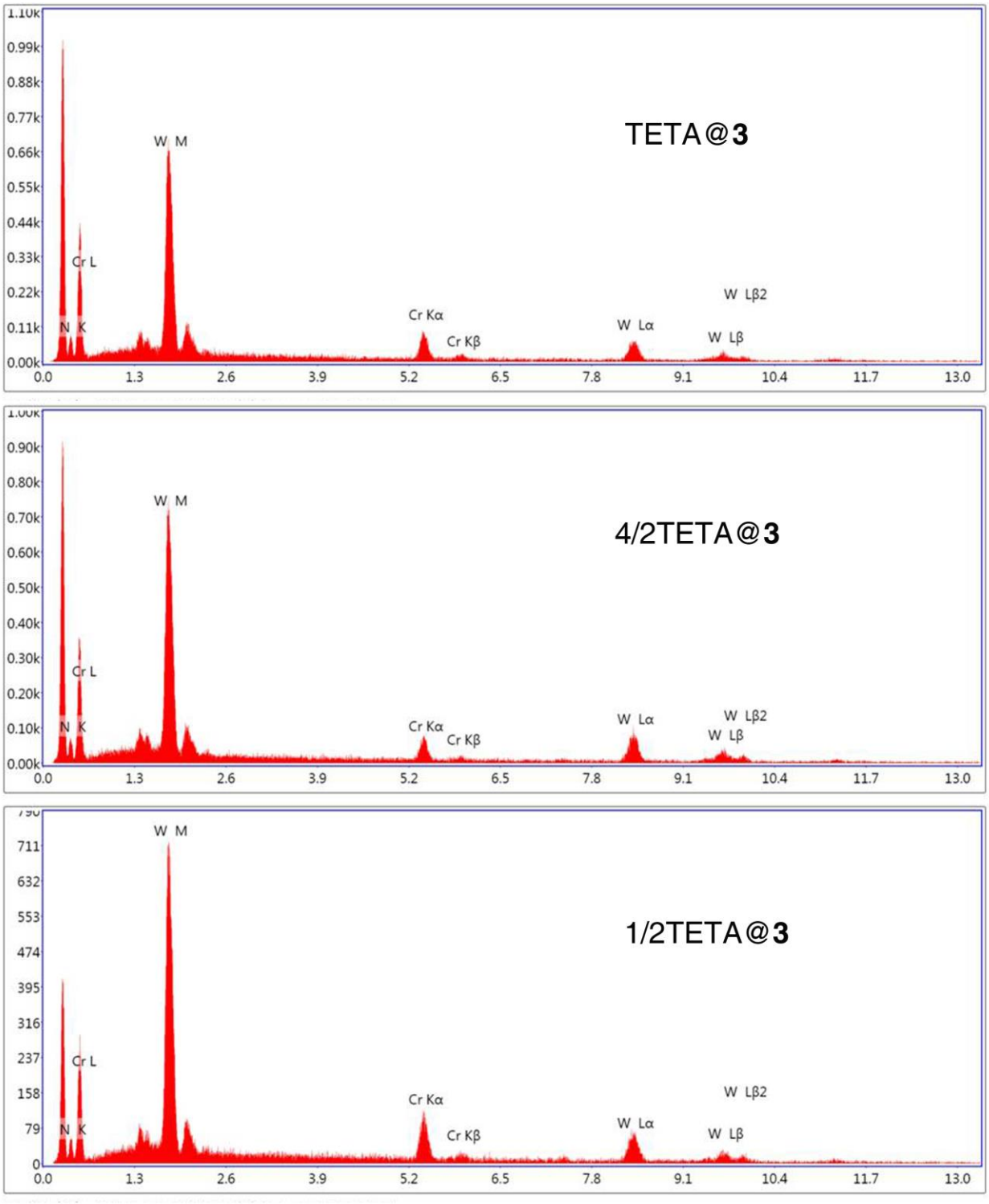

Figure S17. EDX spectrums for TETA@**3**, 4/2TETA@**3**, and 1/2TETA@**3**.

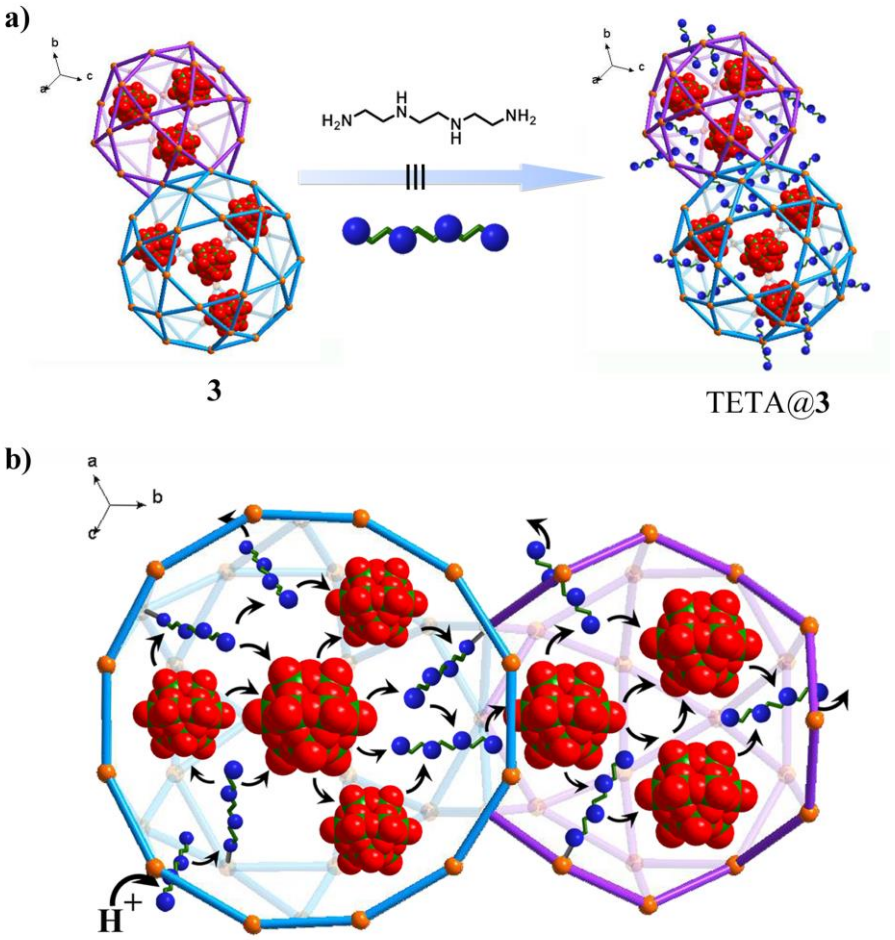

Figure S18. a) Schematic illustration for the preparations of TETA@**3**. b) The possible proton-conducting behaviors in TETA@**3** under 100% RH (H_2O has been omitted in the model for clarify).

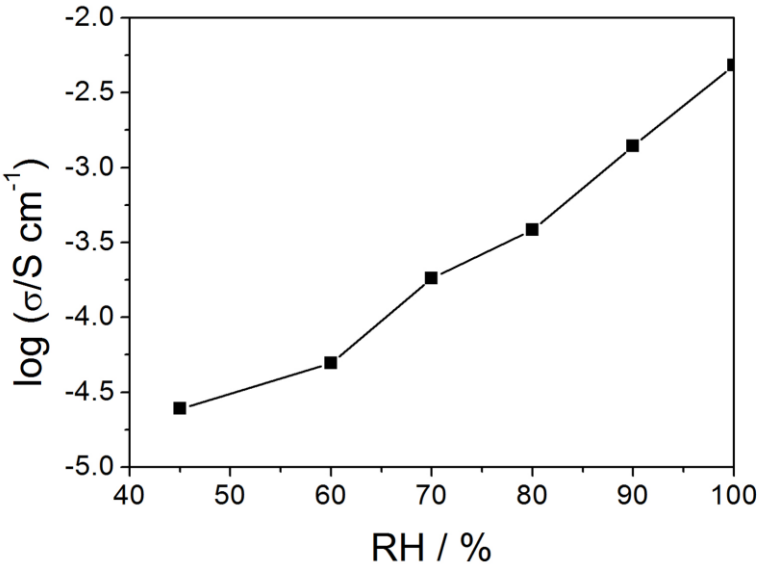

Figure S19. RH dependence of proton conductivity in TETA@**3** at 25 °C.

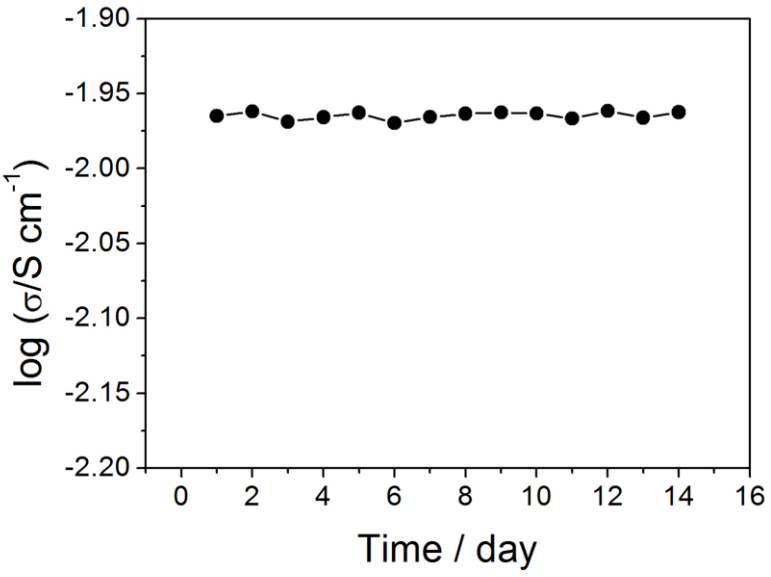

Figure S20. Time dependence of conductivity of TETA@**3** at 80 °C and 100% RH.

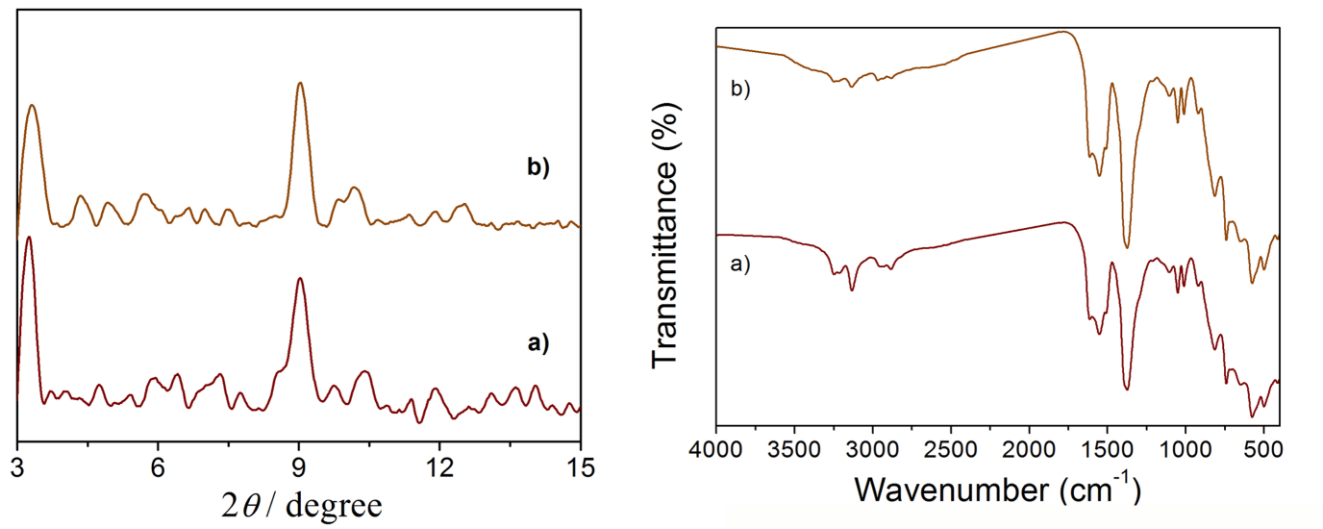

Figure S21. PXRD patterns (left) and IR spectra (right) of TETA@**3** before a) and after b) the impedance measurement.